OXFORD

SOT | Society of Toxicology
www.toxsci.oxfordjournals.org

TOXICOLOGICAL SCIENCES, 169(1), 2019, 151–166

doi: 10.1093/toxsci/kfz029
Advance Access Publication Date: January 29, 2019
Research Article

Propagation of Pericentral Necrosis During Acetaminophen-Induced Liver Injury: Evidence for Early Interhepatocyte Communication and Information Exchange

Ryan C. Kennedy,[*] Andrew K. Smith,[*] Glen E. P. Ropella,[†] Mitchell R. McGill,[‡] Hartmut Jaeschke,[§] and C. Anthony Hunt[*,1]

[*]Department of Bioengineering and Therapeutic Sciences, University of California, San Francisco, California 94143; [†]Tempus Dictum, Inc., Milwaukie, Oregon 97222; [‡]Department of Environmental and Occupational Health, Fay W. Boozman College of Public Health, University of Arkansas for Medical Sciences, Little Rock, Arizona 72205; and [§]Department of Pharmacology, Toxicology and Therapeutics, University of Kansas Medical Center, Kansas City, Kansas 66160

[1]To whom correspondence should be addressed at Department of Bioengineering and Therapeutic Sciences, University of California, 513 Parnassus Avenue, Health Sciences East 1119, San Francisco, CA 94143. Fax: 415 502 4322; E-mail: a.hunt@ucsf.edu.

ABSTRACT

Acetaminophen (APAP)-induced liver injury is clinically significant, and APAP overdose in mice often serves as a model for drug-induced liver injury in humans. By specifying that APAP metabolism, reactive metabolite formation, glutathione depletion, and mitigation of mitochondrial damage within individual hepatocytes are functions of intralobular location, an earlier virtual model mechanism provided the first concrete multiattribute explanation for how and why early necrosis occurs close to the central vein (CV). However, two characteristic features could not be simulated consistently: necrosis occurring first adjacent to the CV, and subsequent necrosis occurring primarily adjacent to hepatocytes that have already initiated necrosis. We sought parsimonious model mechanism enhancements that would manage spatiotemporal heterogeneity sufficiently to enable meeting two new target attributes and conducted virtual experiments to explore different ideas for model mechanism improvement at intrahepatocyte and multihepatocyte levels. For the latter, evidence supports intercellular communication via exosomes, gap junctions, and connexin hemichannels playing essential roles in the toxic effects of chemicals, including facilitating or counteracting cell death processes. Logic requiring hepatocytes to obtain current information about whether downstream and lateral neighbors have triggered necrosis enabled virtual hepatocytes to achieve both new target attributes. A virtual hepatocyte that is glutathione-depleted uses that information to determine if it will initiate necrosis. When a less-stressed hepatocyte is flanked by at least two neighbors that have triggered necrosis, it too will initiate necrosis. We hypothesize that the resulting intercellular communication-enabled model mechanism is analogous to the actual explanation for APAP-induced hepatotoxicity at comparable levels of granularity.

Key words: drug-induced liver injury; hepatic zonation; model mechanism; simulation; systems modeling; virtual experiment.

Acetaminophen (APAP) within its therapeutic range is safe but can produce pericentral (PC) hepatic necrosis in humans and animals when overdosed. To better understand and explain the causes and consequences, it has been studied for decades as a model hepatotoxicant in animals. A characteristic early feature in mice is that necrosis, preceded by covalent adduct formation, begins adjacent to the central vein (CV) and progresses periportally.

A long-standing explanation for the zonation of necrosis in APAP hepatotoxicity is that increasing periportal (PP) to PC production of NAPQI (*N*-acetyl-*p*-benzoquinone imine) is sufficient to explain early PC necrosis. Challenging that explanation in mice is impracticable. Smith *et al.* (2016) endeavored to circumvent the challenges of the *in vivo* mouse model by developing and experimenting on model mechanisms of APAP-induced hepatotoxicity within virtual mice. One, named the NZ-Mechanism, is a parsimonious, somewhat coarse grain instantiation of the NAPQI zonation theory. Measurements of APAP hepatic disposition and metabolism recorded during execution are quantitatively and qualitatively similar (biomimetic) to reported observations within and across several biological levels. Despite substantial zonation of NAPQI production, average early triggering of necrosis occurred first PP and not PC. The results provide strong evidence that NAPQI zonation alone is insufficient to explain early PC necrosis. A somewhat finer grain explanation would be required to cause early PC necrosis.

Starting with the NZ-Mechanism, we created two new model mechanisms by inscribing zonation of one additional feature in each. The GNZ-Mechanism specified that GSH Depletion Threshold values decrease PP to PC. The MNZ-Mechanism specified that a virtual hepatocyte's ability to mitigate the (mitochondrial) damage that triggers necrosis diminishes PP to PC. Results of experiments employing those Mechanisms showed that, early triggering of necrosis was shifted toward the CV, but not sufficiently. The average early location was midzonal and not PC. However, when the two mechanisms were merged to form the MGNZ-Mechanism, average early triggering of necrosis occurred PC. We argued that, at corresponding degrees of granularity, the essential features of the MGNZ-Mechanism and the actual APAP-induced hepatotoxicity mechanism in mice may be strongly analogous within and across multiple lobular levels (Smith *et al.*, 2016).

Experiments using the MGNZ-Mechanism focused on improving a mechanism-based explanation for early features of APAP-induced hepatotoxicity and employed prespecified qualitative and quantitative target attributes. However, if we make the criteria for achieving a target attribute more stringent, the MGNZ-Mechanism may no longer be adequate—it would be falsified. Re-engineering would then be needed to achieve the revised set of targeted attributes. Consider imposing two new target attributes: (1) the earliest necrosis trigger events must occur first adjacent to CV, and (2) subsequent early necrosis trigger events must occur primarily adjacent to virtual hepatocytes (vHPCs) that have already triggered necrosis. The new target attributes help falsify the MGNZ-Mechanism. Virtual experiments employing the MGNZ-Mechanism exhibited few early necrosis trigger events directly adjacent to CV, and many early trigger events were isolated from each other, dispersed among other virtual hepatocytes in a heterogeneous pattern.

The objective of this research is to impose the above two more stringent attributes as simulation targets and seek reasonably parsimonious enhancements to the MGNZ-Mechanism—Control mechanism hereafter—that would enable meeting both. The search for plausible improvements could begin at either the intracellular level or the cell behavior level. We explore both but focus on the latter motivated by two considerations. (1) Evidence supports that intercellular communication via exosomes (Hirsova *et al.*, 2016), gap junctions (Asamoto *et al.*, 2004; Decrock, *et al.*, 2009), and connexin hemichannels (Maes *et al.*, 2017) plays various roles in determining toxic effects of chemicals, facilitating or counteracting the cell death process. (2) The mechanism and software re-engineering required to add communication-enabled rule-based capabilities to the Control mechanism were expected to be modest.

We discovered a pair of rules that require knowledge of whether a downstream or lateral neighbor has triggered necrosis to determine whether a stressed virtual hepatocyte triggers necrosis. We present the results of virtual experiments in which virtual mice (Figure 1) employed a modified version of the Control mechanism (Figure 2) and utilized that pair of rules to achieve both new target attributes. We hypothesize that the resulting intercellular communication-enabled model mechanism is analogous to the actual explanation for APAP-induced hepatotoxicity at comparable levels of granularity.

MATERIALS AND METHODS

We experiment on two kinds of virtual Mice. Control Mice utilize previously validated spatiotemporal model mechanisms (see Requirements) that simulate characteristic early features of APAP hepatotoxicity (Smith *et al.*, 2016). Virtual hepatocytes within Control Mice are quasi-autonomous agents; they do not communicate with neighboring vHPCs. The objective for this work was to discover a reasonably parsimonious set of mechanism enhancements that would enable APAP-induced necrosis in Test Mice to always occur first adjacent to the CV and then spread outward in the PP direction, while continuing to achieve the original Similarity Criteria. To limit confusion hereafter and distinguish virtual Mouse components, characteristics, and phenomena from real mouse counterparts, we capitalize the former and, in some cases, append the prefix v to the object's name. Names of model mechanism features and specifications (parameters) are italicized.

Technical Details

The Java-based MASON multiagent toolkit framework serves as the basis for virtual Mice and many of the model mechanism components (Luke *et al.*, 2005). In earlier work, we referred to virtual Mice as Mouse Analogs (Liver Analogs, Hepatocyte Analogs, etc.) to stress the fact that model mechanism entities (Hunt *et al.*, 2018) are intended to be strongly analogous to their biological counterparts, yet not to model the biology precisely. We utilize agent-oriented modeling methods and techniques (Hunt *et al.*, 2013; Macal and North, 2010). Agent-oriented modeling methods allow for complex software entities (agents) which can implement their own rules and schedules, and which therefore can be made biomimetic in multiple ways. Hunt *et al.* (2018) characterize the spectrum of mechanism-oriented model types being used to help explain biological phenomena. They distinguish three broad types: mechanistic explanation, an analogous mechanism model, and a model mechanism. This work is an example of the latter. We use agent-oriented methods and components to make the model mechanisms utilized by Control and Test Mice concrete and biomimetic. Consequently, mappings exist between the model mechanism's discrete entities and activities, as well as biological counterparts. The expectation is that measurements of a phenomenon generated during execution of a computational model mechanism would adequately match measurements of the actual target phenomenon, within some tolerance, qualitatively and quantitatively.

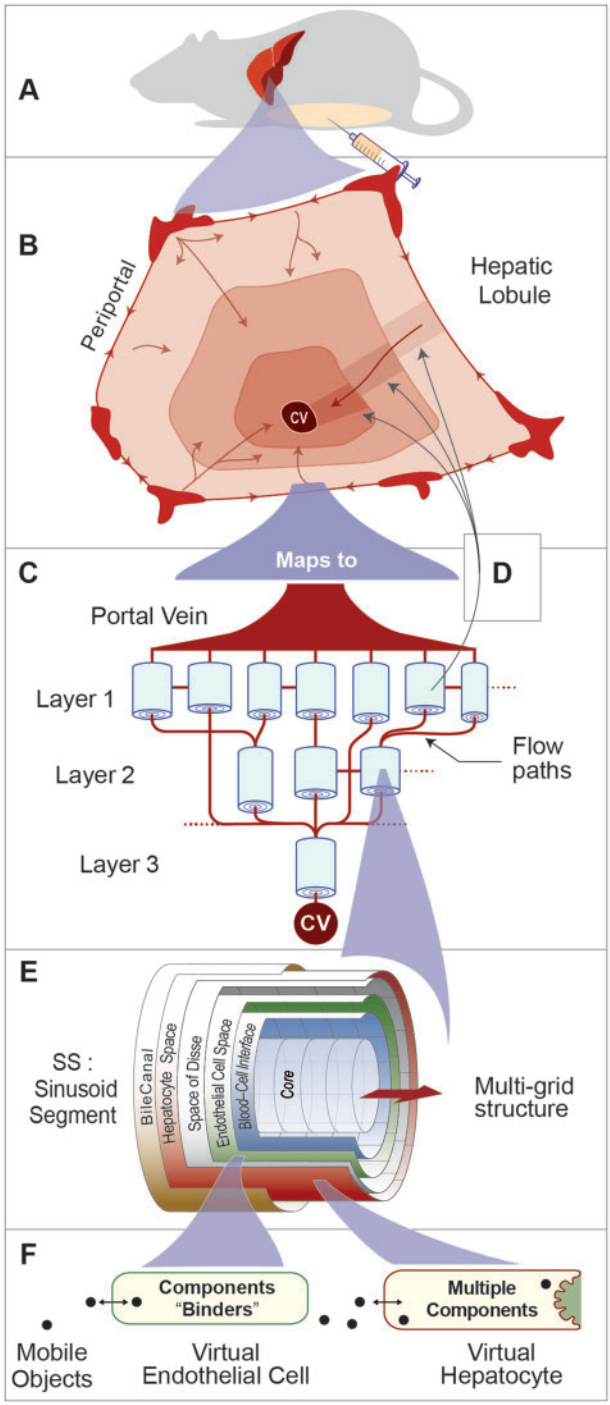

Figure 1. Virtual Mouse components and their organization. A, A virtual Mouse comprises a Liver, Mouse Body, as well as a space to contain Dose for simulating intraperitoneal dosing. B, An illustration of a sectioned hepatic lobule. Different shading illustrates idealized zonation. C, An illustration of a portion (only 16%) of one Monte Carlo-sampled Lobule. D, One Sinusoid Segment (SS) maps to a portion of a lobule, within one of the three illustrated Layers. E, An illustration of a multi-layered SS. F, Virtual Cell objects occupy 99% of the Endothelial Cell space and all of the Hepatocyte space.

We refer to one execution of virtual Mouse software as a trial simulation (simply trial, hereafter). Most events occurring during a trial are stochastic. Numbers of several entities and values

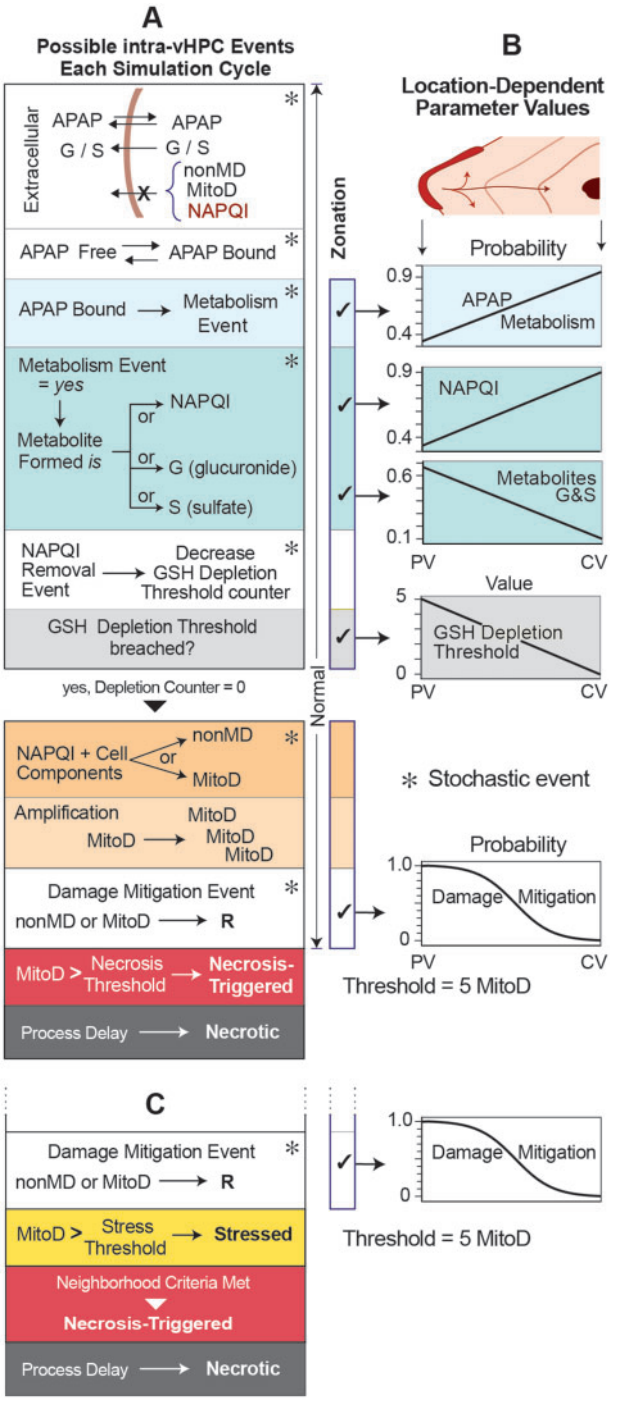

Figure 2. Intrahepatocyte events initiated by APAP. A, Within Control Mouse vHPCs, these events and activities may execute each simulation cycle. They do so independently in a pseudo-random order. Events marked with an asterisk are stochastic. Right side check marks designate features that are subject to Zonation. B, These five graphs show how particular features depend on Lobular location. Left side: the value assigned to vHPCs adjacent to the Portal Vein (PV) entrance. Right side: the value assigned to vHPCs adjacent to the central vein (CV). C, Within Test Mouse vHPCs, the Stressed and Necrosis-Triggered features replace Necrosis-Triggered in Control Mice. Initiation of Necrosis-Triggered is changed to initiation of Stressed (the Threshold value is unchanged). Information about the status of neighbors is used to determine when Necrosis-Triggered may be initiated. Damage mitigation and all other upstream features are unchanged from A.

governing the occurrence of specific activities are Monte Carlo sampled during the simulation, ie, the specific value for that trial is determined by a (pseudo) random draw from a prespecified distribution. Probabilities governing most stochastic events are stated in the specifications. The probability assigned to each stochastic event in Figures 2A and 2B was arrived at during Iterative Refinement (IR) Protocol cycles (described below) as detailed previously (Smith et al., 2014, 2016). The default probability value is .5. It is used for any stochastic event for which the wet-lab evidence is insufficient or too uncertain to guide or justify selecting a different value. We continue using a default probability until a model mechanism failure forces a change.

Most phenomena generated by Control and Test Mice are relatively insensitive to moderate changes to any one event probability value. However, moderate changes to several event probability values can cause noticeable changes in one or more generated phenomena.

The R programming language was used to facilitate analysis and to plot experiment measurements. Virtual Mice and specification files are managed using the Subversion version control tool in two repositories, one private (Assembla) and another public. All specification values for Control vHPCs are the same as used previously by Smith *et al.* (2018). Values for crucial Control and Test vHPC specifications are listed in Supplementary Table 1. Our entire toolchain is open source. The data presented herein along with the code are available from project websites (https://simtk.org/projects/aili; last accessed February 19, 2019 and https://simtk.org/home/isl/; last accessed February 19, 2019).

Histology

Male WT C57Bl/6J mice were purchased from the Jackson Laboratory (Bar Harbor, Maine). The mice were used for experiments at 8–12 weeks of age. Animals were housed in a temperature-controlled facility with a 12 h light/dark cycle and allowed *ad libitum* access to food and water. Food was withdrawn 12–16 h before treatment with 300 mg/kg APAP. APAP was dissolved in warm 1× phosphate-buffered saline and injected i.p. Liver tissue was harvested at 0, 1, 2, 3, 4.5, and 6 h post-APAP. A piece of each liver was fixed in 10% phosphate-buffered formalin and then embedded in paraffin wax. Sections (5 μm thick) from each liver were stained with hematoxylin and eosin (H&E) for histology. Additional sections were stained for DNA fragmentation using a terminal deoxynucleotidyl transferase dUTP nick-end labeling (TUNEL) kit from Roche (Indianapolis, Indiana), as described previously (Gujral *et al.*, 2002). All animal protocols were approved by the Institutional Review Boards or the University of Kansas Medical Center and the University of Arkansas for Medical Sciences.

Virtual Mice: Structure and Function

Figure 1 illustrates a virtual Mouse, which consists of a Body, a Liver, and a space for the virtual acetaminophen (vAPAP) dose. We developed the Liver using an IR Protocol (discussed below) and by adhering to strong parsimony guideline: resist adding plausibly more realistic detail until it is needed to achieve a particular attribute or validation target. During each trial, phenomena generated are qualitatively and quantitatively analogous to actual wet-lab counterparts across several metrics. It met target attributes in six studies (Park et al., 2009, 2010; Smith et al., 2014, 2016; Yan *et al.*, 2008a,b). The Liver has a specified number of Monte Carlo-determined Lobule variants. One Lobule maps to a small random sample of possible lobular flow paths within a whole liver, and reflects the fact that APAP in blood entering portal vein (PV) tracts gets exposed to many more hepatocytes than does APAP in blood exiting the CV. A virtual Lobule (Figure 1C) is a directed graph with a Sinusoidal Segment (SS) agent at each node. Flow follows the directed graph. We organize graph nodes into three Layers, which map to three lobular zones. There are 45 nodes in Layer 1, 20 in Layer 2, and 3 in the third Layer. That structure maps directly to the quasi-polyhedral nature of hepatic lobules. In Control Livers, all SS dimensions are Monte Carlo determined within constraints that enabled achieving previously described Target Attributes. SS dimensions in Layers 1 and 2 are Monte Carlo determined as in Control Livers. However, the circumferences of all Layer 3 SSes are 30 grid spaces and the lengths are 8 grid spaces.

The 45/20/3 ratio of directed graph nodes in Layers 1–3 does not represent relative amounts of tissue in 3 acinar zones. The number and arrangement of graph nodes along with SS dimensions came from challenging various graph topologies using the IR Protocol (below). That arrangementprovided the variety of flow paths needed to achieve quantitative liver perfusion and hepatic disposition validation targets for several drugs in normal and diseased rat livers (Hunt *et al.*, 2006; Park *et al.*, 2009; Yan *et al.*, 2008a,b); it maps adequately to relative lobular volumes. There is a chance that some virtual experiment results may change in subtle ways if small changes are made to graph topology. However, our sensitivity studies have not shown such changes.

A SS comprises a Core, Blood-Cell Interface, Endothelial Cell Space, Space of Disse, Hepatocyte Space, and Bile (not a factor for this work). Events occurring within a particular SS are strongly analogous to referent events within portions of sinusoids and adjacent tissue. vAPAP, its Metabolites, and other virtual Compounds (vCompounds) are mobile objects. A vAPAP maps to a tiny fraction of an APAP Dose, which for these experiments is 45 000 objects. Mobile objects from Mouse Body are first delivered to the PV. Extra-Cellular mobile objects percolate stochastically through accessible spaces toward the CV influenced by specifications that control local flow. Mobile objects exit a Layer 3 SS into the CV and then get moved to the Body. PV-to-CV gradients provide intra-Lobular location information to each vHPC.

Each Cell is a software agent. Cells in Endothelial space control vAPAP entry and exit and contain a probability-specified number of Binders; they merely bind and release vAPAP and map to a conflation of all epithelial cell components responsible for nonspecific vAPAP binding.

Control Mice: Intrahepatocyte Model Mechanisms

vHPCs within a Control Mouse Liver utilize the Control mechanism illustrated in Figures 2A and 2B. Entry and exit of mobile objects from each Endothelial Cell and vHPC are mediated by the Cell, according to the vCompound's properties. On average, there are 16 165 vHPCs per Lobule. Objects within vHPCs and their capabilities are identical to those used previously (Smith et al., 2016). The event descriptions that follow are per simulation cycle. vHPCs contain four types of physiomimetic event management modules (Petersen et al., 2014) to control material entry and removal along with binding and the object transformations described in Figure 2: *MetabolismHandler*, *BindingHandler*, *InductionHandler*, and *EliminationHandler* (the last two are not used in this work). The order of events is (pseudo) randomized during each simulation cycle.

There is a direct mapping between the probability of a vAPAP Metabolism event and the amount of metabolic enzymes. The probability of a vAPAP Metabolic event and the probability that the Metabolite is NAPQI each increase 3-fold

from PV entrance to CV. All other metabolites are lumped together and divided equally between G (maps to APAP glucuronide) and S (maps to the APAP sulfate metabolite). Each of the 5 gradients in Figure 2B is implemented explicitly as a function of distance from PV entrance to the vHPC's position. Each vHPC uses a location-dependent value drawn from those gradients. We represent the futile cycle in which APAP is deacetylated to para-aminophenol followed by rapid reacetylation back to APAP, even though the cycle has been viewed as having little importance in APAP-induced hepatotoxicity in humans and mice (Miyakawa *et al.*, 2015).

The probability during each simulation cycle that a NAPQI is removed (maps to undergoing a reaction) is .5. Each vHPC is assigned a location-dependent value for its GSH Depletion Threshold. Before the Threshold is breached, and once a NAPQI is created, it is eliminated 90% of the time, and the GSH Depletion accumulator is incremented by 1.0, which maps to depleting a fraction of a hepatocyte's available GSH. However, 10% of the time, the NAPQI object remains in the vHPC. The Threshold is breached when the accumulator value exceeds the vHPC's GSH Depletion Threshold value, which maps to GSH depletion. In each cycle, there is a 50% chance that a NAPQI object will be removed and that one of the two types of Damage product will be added to that vHPC: a mitoD object maps to a conflation of a fraction of all mitochondrial damage products; a nonMD object maps to a conflation of a fraction of all other types of damage products. The granularity of mitoD in the above process proved to be insufficient to simulate downstream toxicity events. Mindful of our strong parsimony guideline, we amplify mitoD formation: we specify that one NAPQI $\rightarrow (1+n)$ mitoD. Without wet-lab data for guidance, we specified n to be a pseudo-random draw from a Gaussian distribution with $\bar{x}=4$, $SD=1$. Such mitoD amplification can also map to the accumulation of reactive oxygen/nitrogen species.

We assume that hepatocyte death always follows triggering of necrosis. Once the amount of accumulated mitoD exceeds the Necrosis Threshold, the Necrosis-Triggered state is induced. Further, because necrosis is a process, there is a delay between the triggering event and when necrosis becomes detectable in stained tissue sections. Within Control and Test Mice, for each vHPC, that delay interval is a pseudo-random draw from a uniform distribution [Max, Min] that is specified by *necrosisDelay[Max, Min]*. There is considerable uncertainty about the timings of triggering events and histological confirmation of necrosis. And there is no evidence of necrosis occurring by 1 h. Smith *et al.* (2016) use *Min* = 1.2 h (4320 simulation cycles) and *Max* = 12 h (43200 cycles). For simplicity and clarity of results, we use *Min* = 1.39 h (5000 cycles) and *Max* = 5001 cycles.

In vivo hepatocytes utilize multiple mechanisms to mitigate or reverse damage. Consistent with our parsimony guideline, we implemented a single mitigation mechanism, repurposing a Metabolism Module, and named it Damage Mitigation. It maps to a conflation of all actual mitigation/recovery/macromolecular repair mechanisms, including removal of acetaminophen-protein adducts by autophagy (Ni *et al.*, 2016). With a location-specified probability, a Repair object replaces a Damage product. We focused on mitoD because only its biological counterpart can trigger Necrosis. Specifying that the probability of a mitoD Mitigation event decreases sigmoidally PV-to-CV enabled Necrosis-Triggered events to occur first close to—but not at—the CV in the Control mechanism, as documented in Results, and is consistent with the observation that zonated induction of autophagy limits APAP-induced necrosis (Ni *et al.*, 2013).

Requirements

To achieve the objective, we utilize the virtual experiment protocol outlined by Kirschner *et al.* (2014), as updated by Smith *et al.* (2016) and Petersen and Hunt (2016). We adapted this definition of a mechanism from Darden (2008) and Illari and Williamson (2012) as applied to generation of a biological phenomenon: entities and activities organized and orchestrated in such a way that they are responsible for the phenomenon to be explained. All features of Control and Test model mechanisms during operation meet that definition. Thus, Control and Test model mechanisms are concrete hypotheses for how features of APAP hepatotoxicity in mice are generated. Five requirements are specified to guide software engineering, mechanism instantiation, and simulation refinements. (1) Virtual entities are concrete and biomimetic in prespecified ways. (2) Model mechanism features during each trial are measurable. (3) Specific feature measurements match or mimic (ie, are strongly analogous to) prespecified Targeted Attributes, but only to the extent needed to achieve the Similarity Criteria. (4) Higher-level phenomena arise during each trial from concrete component interactions at a lower level. (5) Present arguments that, during each trial, at a comparable level of granularity, the model mechanism has a biological counterpart.

Limits on Mappings

Lobules are not designed to map directly to hepatic lobules and a SS does not map directly to a portion of a single sinusoid surrounded by hepatic endothelial cells and hepatocytes. Instead, a Lobule maps to a small random sample of possible lobular flow paths within a whole liver. The mapping from cylindrical 2D Hepatocyte Space to corresponding 3D configurations of hepatocytes is indirect and not intended to be literal. Instead, for its function as a component of a model mechanism, it is intended to be adequately analogous. We sought a balance between the computation programmed into the objects and their methods. Lobule design does enable measurements of the Hepatic Disposition and Metabolism of vCompounds during virtual Liver perfusion experiments—averaged over many Monte Carlo trials—to validate quantitatively to temporal measurements of referent compounds made during liver perfusion experiments.

Iterative Refinement Protocol

Starting with a verified copy of Control Mouse code, achieving the objective required making and testing incremental changes to model mechanism features and their specifications. Each step of the process followed a version of the IR Protocol (Hunt *et al.*, 2009), which is a best practice for developing scientifically useful model mechanisms (Petersen *et al.*, 2016; Smith *et al.*, 2016). Each execution generates predictions that are tested or challenged during an IR Protocol cycle. The goal of an IR Protocol cycle is to test whether, during each trial, a simulation feature will mimic a target attribute at a specified tolerance. Failure to do so falsifies the current model mechanism. Overcoming such failures improves explanatory insight and credibility. There are six key IR Protocol cycle steps. (1) State the cycle's objective. (2) Specify Target Attributes and Similarity Criteria. (3) Specify granularity for the updated model mechanism. (4) Revise mechanism in small steps, while adhering to a strong parsimony guideline. Record reasoning for modifications, and create a revision plan. (5) Evaluate the results of virtual experiments designed to evaluate revisions; and (6) Determine if Target Attributes have been achieved. If not, offer

a plausible explanation and corrective strategy, and start a new IR Protocol cycle.

Building the Credibility of Virtual Mice

Test mice are works in progress. They are a stage in the larger effort of developing improved models of explanation for features of APAP-induced hepatotoxicity. The virtual experiments described herein provide an explicit way of incrementally connecting (or not) a putative explanatory model mechanism to a phenomenon of interest. During each stage, validation, falsification, verification, and prediction efforts contribute differently to building the credibility of evolving mechanism-based explanations.

Prediction. In science, explanations are usually inductive. Ideally, explanation precedes prediction, permitting deductive reasoning (Mulugeta *et al.*, 2018). Each virtual Mouse execution generates predictions, some of which are selected for testing during the next IR Protocol cycle. However, the focus is on improving the mechanism-based explanation. When needed or justified, it is straightforward to use the tuneable resolution approach (Kirschner *et al.*, 2014) to add details that improves apparent realism (eg, see Pogson et al., 2006). However, we aim to keep Control and Test Mouse mechanisms parsimonious in order to retain scientific usefulness. As explanatory credibility increases, an additional effort can be invested in achieving more precise predictions of hepatotoxicity features.

Validation and falsification. Virtual Mice are both structural and behavioral hypotheses for corresponding mouse experiment features. The phenomena generated and the events occurring during an execution are features of a concretized mechanism-based explanatory hypothesis. As such, validation methods include both explanatory and predictive types, and are both qualitative and quantitative. Because Test Mice are instantiated hypotheses, failed IR Protocol cycles indicate a flawed aspect of the instantiated hypothesis. Successive IR Protocol cycles aim to overcome that failure. Thus, in advancing the science, validation is just one part of an ongoing two-part process. Falsification is the essential second part. Increasing Similarity Criteria or adding new Target Attributes (as done here) can falsify a model mechanism. We demonstrate herein that an essential part of increasing credibility is planning the falsification of the current best explanation. Protocols for mechanism hypothesis testing are those used previously (Smith *et al.*, 2014, 2016). They involve pairing a qualitative or quantitative measurement with well-defined Similarity Criteria. Each pairing requires consideration of two aspects of the Target Attribute: (1) similarity between measurements of a Test Mouse's phenomenon and measurements of the corresponding wet-lab phenomenon, and (2) similarity of variability within and between repeat virtual and wet-lab measurements. Because events occurring during an execution are concretized, specific events and features can be singled out as potential future validation targets (but otherwise may not be recognized as such).

Verification. Using pseudo-random generators facilitates verification. Because virtual Mice constitute concrete structural mechanism hypotheses, verification is most straightforward for mathematically well-defined subcomponent requirements. Unit tests for those use cases are included side by side with the components in the repositories. Integrated verification is performed traces, self-consistency, and face validation with the comparison of the expected against the measured systemic impact of a new or modified component.

Two Divergent Approaches

We imposed two additional target attributes: the earliest Necrosis-Triggered events occur first adjacent to the CV, and subsequent Necrosis-Triggered events occur primarily adjacent to vHPCs that have already Triggered Necrosis. There is a spectrum of Control mechanism variants that can be used to begin achieving both new target attributes plus those already achieved. We began at the parsimonious end of the spectrum and explored two divergent approaches: (1) keep vHPCs quasi-autonomous and focus on making intra-vHPC events (Figure 2) incrementally more interconnected and detailed, consistent with available evidence. (2) Alternatively, in Test Mice, emphasize inter-vHPC communication and acquisition of neighbor status information. Hepatic reality likely involves both, but the IR Protocol stresses an incremental approach in which we resist adding plausibly more realistic detail until it needs to achieve a particular attribute or validation target. We limit attention to the first 6 h following the vAPAP dose and do not consider enhancements that require time-dependent Mechanism changes, such as Enzyme induction (Ropella *et al.*, 2009), although such enhancements are expected to become necessary as we begin explaining additional phenomena beyond 6 h. For example, evidence indicates that, as stress declines pericentrally 6–12 h post-dose, adaptive responses to cellular stress, including mitophagy and mitochondrial biogenesis, become increasingly influential (Du *et al.*, 2017; Ni *et al.*, 2013).

The approach for option (2) is presented in the next subsection. For option (1) we considered several refinements of particular events in Figure 2A. To merit exploration, we required preliminary evidence that a refinement would skew Necrosis-Triggered events toward the CV. One was successful, and it involved linking mitoD amplification and the GSH Depletion Threshold. Within Control Mice, mitoD amplification is independent of location and the number of GSH Depletion events. We specified that breaching the GSH Depletion Threshold be a requisite for mitoD amplification. Doing so makes mitoD amplification location dependent. An option for future consideration is upregulation of Damage Mitigation triggered by accumulating a minimum amount of Damage. The current coarse grain Damage Mitigation events subsume fine grain subprocesses such as mitophagy and mitochondrial biogenesis.

Acquiring and Using Information About Neighbors

Despite the above mapping limitations, we reasoned that enhancing the Control model mechanism by requiring an exchange of information among neighboring vHPCs within the same SS could serve as biomimetic analogies of *in vivo* counterparts. Our initial premise was that information provided through interhepatocyte communication is necessary for establishing the characteristic spatial patterns of APAP-induced necrosis. We assumed that information exchange among neighboring hepatocytes is a continuous process, and speculated that so long as a hepatocyte is capable of recovering from toxin-induced injuries, communication continues.

We specified that a vHPC could obtain information only about neighbors residing in a predefined Moore or von Neumann neighborhood. We posed this question: without changing the pre-Necrosis Trigger model mechanisms in Figure 2A, can we discover a plausible combination of rules that each vHPC must follow, and in doing so, can we achieve our objective, ie, Necrosis-Triggered in Test Mice always occurs first

adjacent to CV and then spreads in the PP direction? If doing so is problematic, that would falsify one or more features of the Figure 2A model mechanisms. By achieving our objective, we can argue that analogous processes may occur *in vivo*. Further, a discovery of such logic would provide a fresh mechanism-oriented perspective for improving explanations of patterns of APAP-induced hepatic injury.

We conjectured that hepatocytes *in vivo* that are close to the CV, especially those adjacent to the CV, are aware of their unique location. To provide Test vHPCs with similar information, we added the new *Adjacency* feature to each vHPC. Specifying *Adjacency* = 0 means the vHPC is directly adjacent to the CV. The adjacency information is needed to step through the logic (described in Results). Upon execution, each vHPC queries its SS grid to establish its location. Each SS grid point is defined by an *x*- (circumference within grid) and *y*-value (direction of flow). A particular vHPC identifies the location of its neighbors by comparing a neighbor's *y*- and *x*-values to its own. During each simulation cycle, each member of the neighborhood is queried for its status.

For early IR Protocol cycles, we relied on MASON's built-in methods for all neighborhood calculations, including the toroidal method that wraps each SS 2D grid to mimic a cylinder. However, wrapping appeared to go beyond the origin, and that caused extraneous neighbors counting downstream von Neumann or Moore neighbors. To avoid that problem, we added logic to specify when wrapping is allowed during that determination. Doing so enabled us to count downstream neighbors more explicitly.

Pericentral Snapshot Animations

We implemented an SS visualization method, hereafter PC Animations. Studying PC Animations facilitates evaluating spatiotemporal changes in vHPC status—Normal, Stressed, Necrosis-Triggered, and Necrotic—among Layer 3 SSes, and aids verification following each implementation change. During each trial, at the end of each simulation cycle, if one or more vHPCs changed status during that simulation cycle, then a snapshot was recorded and time-stamped. It identified the status of all vHPCs in the SS at the end of that cycle. We strung together in sequence all the snapshots from each Layer 3 SS during one trial into a single animation. Observing location-specific temporal changes in status enabled us to identify potentially nonbiomimetic features, and gauge progress.

Measurements

Virtual measurements are made analogous to wet-lab counterparts to facilitate comparisons when wet-lab data are available. Data are measurements of selected vAPAP Disposition, Metabolism, and Toxicity-related phenomena. Because each trial's specification is Monte Carlo determined and the unfolding of events is stochastic, there is considerable variability among measurements from multiple trials governed by the same set of initial specification values. Consequently, results from a single experiment require aggregating measurements across several trials, for which we use the average. For this work, one experiment = 12 Monte Carlo trials. During each trial, each discrete simulation cycle maps to approximately 1 s. In some cases, we measured selected phenomena for each Monte Carlo trial.

During each experiment, for each vHPC, we measured amounts of vAPAP, NAPQI, and mitoD, along with counts of the following events: GSH Depletion, Damage Mitigation, plus initiation of Stressed, Necrosis-Triggered, and Necrotic. They were then summed or averaged for the entire Lobule and within two narrow bands: (1) The PP band includes all 3535 vHPCs that are 4–8 grid points from PV; (2) the PC band includes all 630 vHPCs that are 0–6 grid points from the CV. The average number of vHPCs per Lobule is 16 165, with Layer 1 = 10 860, Layer 2 = 4910, and Layer 3 = 720.

RESULTS

Histology

The histological evidence in Figures 3 and 4 is consistent with that provided in earlier reports (Gujral *et al.*, 2002). All 1 h sections were indistinguishable from control 0 h sections. Some cells in the indicated area of the 2 h section in Figure 3 appear somewhat swollen and pale. Examples of nucleus shrinkage indicate that some hepatocytes are in various stages of pyknosis. At 3 h, many hepatocytes close to CVs appear swollen, and they are losing some basophilic staining. Closer to the CVs, there is evidence of sparse necrosis. By 4.5 h, necrosis occurs, and the area of necrosis is expanding. Pyknosis is more extensive than at 3 h, and karyorrhexis (fragmentation and loss of nuclei) is apparent (which is confirmed by results in Figure 4). By 6 h, karyorrhexis is widespread. There is further loss of basophilic staining, and the areas of necrosis are expanding.

The TUNEL stained sections at 1, 2, and 3 h in Figure 4 reveal no evidence of DNA fragmentation. However, by 4.5 h DNA fragmentation is evident in both the nucleus and the cytosol within clearly defined regions close to the CVs. DNA breakage is a late event in the molecular mechanisms of APAP hepatotoxicity. Given the extent of DNA fragmentation at 4.5 h, as indicated by extensive dark gray staining, the stained material is mostly dead hepatocytes (maps to Necrotic). There is also evidence of DNA fragmentation in several isolated hepatocytes close to the area of extensive PC damage. At 6 h, the area of TUNEL staining is enlarged.

Experiments Using Control Mice

Results of experiments using Control Mice are indistinguishable from earlier results (reported by Smith et al., 2016, 2018). Below, we summarize selected vAPAP disposition and toxicity measurements at the vHPC level to facilitate comparisons with results of experiments using Test Mice.

Results in Figure 5 show that per-vHPC values for vAPAP, NAPQI, GSH Depletion events, Mitochondrial Damage, and Damage Mitigation events within the PC band are larger than corresponding average Lobular values. For NAPQI and Mitochondrial Damage, they are dramatically larger. Lobular values are larger than corresponding values within the PP band. Those striking differences are a consequence of two factors: (1) vHPCs are exposed to vAPAP sequentially, PP-to-PC; (2) the majority of Lobular vHPCs are in SS Layer 1.

The Lobular structure reflects the fact that compounds in blood entering PV tracts get exposed to many more hepatocytes than compounds in blood close to the CV. The Layer 1/Layer 3 vHPC ratio averages 15.1, with 65.9%, 29.8%, and 4.3% of vHPCs in Layer 1, 2, and 3 SSes, respectively. Consequently, despite vAPAP Metabolism in Layers 1 and 2, vAPAP per vHPC in Layer 3 is greater than in Layers 2 and 1. The ratio would be larger except for a mitigating factor: as specified in Figure 2B, the probability of a vAPAP Metabolism event is Layer 3 > Layer 2 > Layer 1. Those PP-to-PC differences help explain why per-vHPC amounts for vAPAP within the PC band are >4× the amounts within the

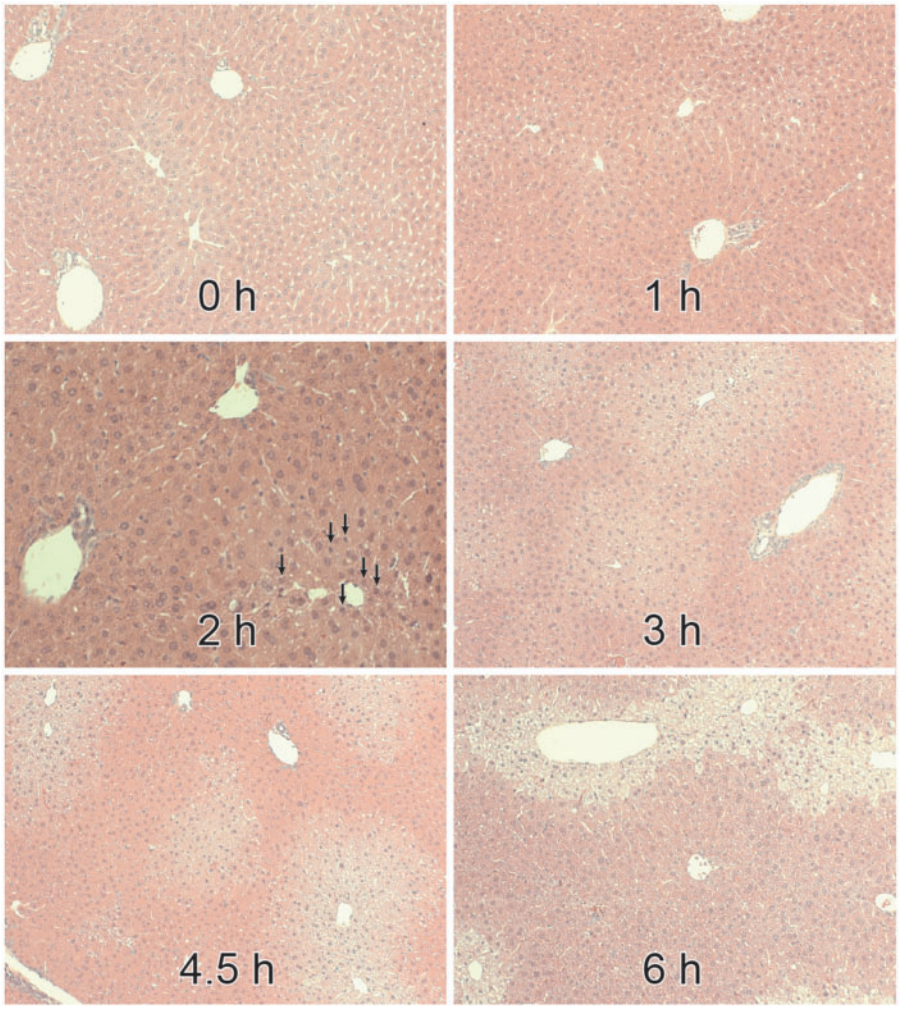

Figure 3. Evidence of pericentral (PC) APAP-induced tissue injury. Shown are representative photomicrographs of liver sections stained with hematoxylin and eosin (H&E) at the indicated times following a 300 mg/kg dose of APAP. The magnification of the 2 h section is 200×; the magnification of the other sections is 100×. Features in the 1 h section are indistinguishable from those in the 0 h section.

PP band (Figure 5A). Upstream Metabolism of vAPAP prevents the difference from being larger.

Because NAPQI formation increases PP-to-PC (Figure 2B), the per-vHPC amounts of NAPQI within the PC band (Figure 5C) are larger than within the PP band. However, cumulative per-vHPC GSH Depletion events within the PC band (Figure 5D) are only about twice those within the PP band. That is in part a consequence of the smaller PC GSH Depletion Threshold (Figure 2B).

The amounts of mitoD within the PP band are insignificant compared with those within the PC band (Figure 5E) because of the probability of a Damage Mitigation event (removal of a mitoD) during each simulation cycle is largest within the PP band (Figure 2B). Greater rates of Damage Mitigation within the PP band limits mitoD accumulation and the cumulative per-vHPC number of Damage Mitigation events within the PP band (Figure 5F) demonstrates that the small amounts of mitoD within PP vHPCs are a consequence of Damage Mitigation, rather the absence of mitoD formation. That feature is consistent with *in vivo* studies demonstrating that mitochondrial dysfunction is widespread and reversible after APAP treatment (Hu *et al.*, 2016). Besides, it has been shown that extensive mitochondrial biogenesis outside the core area of necrosis limits further expansion of the damaged area (Du *et al.*, 2017).

The mean distance from the CVs of Necrosis-Triggered events (Figure 5B) is provided for only 80 min because we are most interested in relative locations of early events. Because of the considerable variance in locations of individual events, the plotted average locations are 181-point moving averages. Figure 5B shows that the average location of Necrosis-Triggered events in Control Mice begins close to but not at the CVs. The average location corresponds to the highest density of Necrosis-Triggered events averaged over many Monte Carlo trials. Density values, which are highly skewed, diminish in the PP direction. There is no clear demarcation between vHPCs that are and those that are not Necrosis-Triggered. Whereas, clear changes in staining pattern are evident at 3, 4.5, and 6 h in Figure 3 and at 4.5 and 6 h in Figure 4.

A Refinement of the Control Mechanism

We experimented to test the hypothesis that relative to results from experiments using Control Mice, requiring that the GSH Depletion Threshold be breached before mitoD amplification can occur will skew the mean location of early Necrosis-

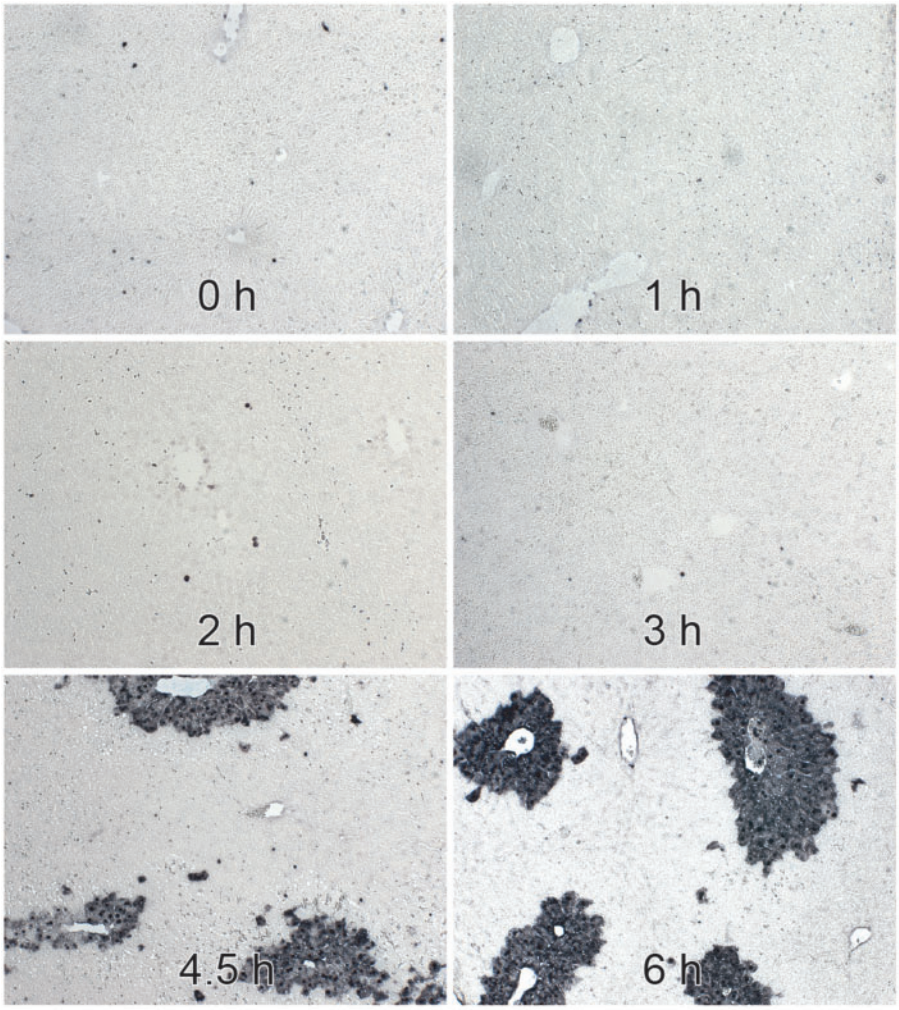

Figure 4. TUNEL staining for visualization of DNA fragmentation. These representative photomicrographs are mouse liver sections from the same experiment as the Figure 3 liver sections. The magnification of all sections is 100×. TUNEL positive cells are dark gray. The 1, 2, and 3 h sections show no evidence of TUNEL staining.

Triggered events toward the CV before spreading in the PP direction. The Mechanism refinement is presented in Supplementary Experiment 7, and results supporting the hypothesis are presented in Supplementary Figure 8. The refinement caused the mean location of all early Necrosis-Triggered events to shift dramatically closer to the CV, and the variance in location of mean Necrosis-Triggered events was reduced considerably. However, there is still no clear demarcation between vHPCs that are and those that are not Necrosis-Triggered.

Test Mice: Logic Development Workflow

The logic diagram in Figure 6 is the end product of the following workflow. We posited that 5 new behaviors would be needed to achieve our objective. (1) Initiation of Necrosis-Triggered does not occur in isolation. (2) Accumulate mitoD Damage Products beyond some threshold value would be insufficient to initiate Necrosis-Triggered; at least one downstream neighbor must have also initiated Necrosis-Triggered. (3) One or more behaviors of vHPCs adjacent to the CV must be unique. (4) To enable the first two behaviors in Test Mice, we changed Necrosis-Triggered status (Control Mice) to Stressed state and Necrosis Threshold to Stress Threshold. (5) In Control vHPCs, when Necrosis Threshold is breached, there is an irreversible transition to Necrosis-Triggered. However, the transition to Stressed should not be irreversible: while Stressed, if mitoD drops below Stress Threshold during a simulation cycle, the vHPC reverts to Normal status.

We began by addressing the first of the above four behaviors. At the conclusion of a Control Mouse experiment (after all NAPQI has been removed), we often see Necrotic vHPCs in Layer 3 that are surrounded by Normal vHPCs. We occasionally see a Necrotic vHPC where the closest Necrotic neighbor is more than two grid points distant. Moreover, we see some Normal vHPCs adjacent and close to the CVs. The following is one of several possible explanations for the latter: because of the stochastic, discrete event nature of the simulations, early accumulation of mitoD within those Normal vHPCs may have been insufficient to breach the Necrosis Threshold. Analogous circumstances may occur *in vivo*, but we see no histological evidence of one or a few normal hepatocytes surrounded by damaged or necrotic neighbors. We conjectured that having damaged or necrotic neighbors may be sufficient to trigger necrosis. To avoid isolated Necrotic vHPCs, we added this rule: if the vHPC has not initiated Necrosis-Triggered, but its von Neumann neighborhood (for Manhattan radius of $r = 2$; illustrated in Figure 6) contains two or more downstream neighbors that have initiated Necrosis-Triggered, then it initiates Necrosis-Triggered. Subsequently, we added the option for the vHPC to use the

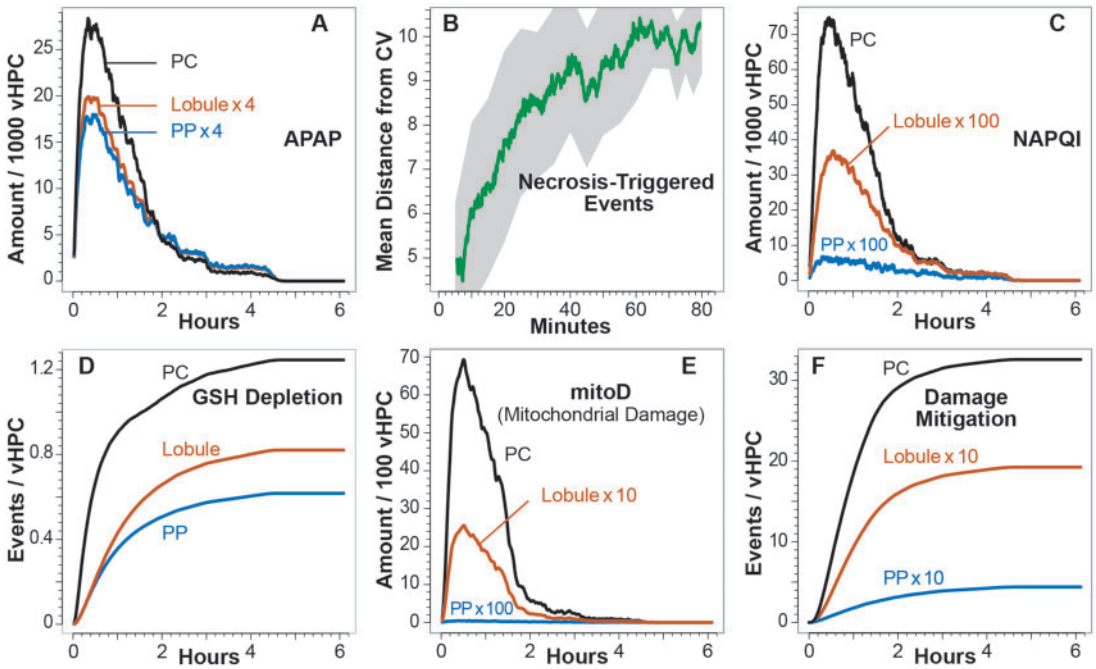

Figure 5. Control Mice: spatiotemporal measurements of intra-vHPC events. Control vHPCs do not communicate. Plotted values in A, B, C, and E are 181-point centered moving averages. A, Values are average amounts of APAP in 1000 vHPCs. Lobule: Lobule-wide averages; PC: average amounts per vHPC in the first six grid spaces adjacent to the CV; and PP: average amounts per vHPC in the 5th-9th grid spaces downstream of the PV entrance. B, Average location each simulation cycle of vHPCs that have initiated Necrosis-Triggered. The gray-shaded area spans ± 1SD at 2.5–5 min intervals. C, Average amounts of NAPQI in 1000 vHPCs for the preceding three locations. D, Total GSH Depletion events per vHPC. E, Average amounts of Mitochondrial Damage in 100 vHPC. F, Total Damage Mitigation (Repair) events per vHPC. For cumulative profiles such as D and F, a repeat experiment would not generate the exact same values.

$r = 2$ Moore neighborhood, because it increased the probability that the vHPC will be influenced by a downstream neighbor that has initiated Necrosis-Triggered. Using that rule caused the average location of Necrosis-Triggered to be further skewed in the CV direction relative to the corresponding Control average locations. However, we observed several early Necrosis-Triggered events at locations more than 5 grid points from the CV, and much later Necrosis-Triggered events adjacent to CV.

Further, as trials progressed, we observed non-Necrosis-Triggered vHPCs forming columnar features "Rising" from the CV. The logic diagram for the preceding implementation, along with revised diagrams for subsequent implementations, are provided in Supplementary Figure 1. Depending on the trial, von Neumann or Moore neighborhoods were used. Von Neumann neighborhoods rely on an interface between vHPCs. For example, a von Neumann neighborhood specified by $r = 1$, encompasses only 4 vHPCs. With $r = 2$, the neighborhood increases to 12. Moore neighborhoods do not require interfaces. They include all vHPCs surrounding the decision-making vHPC. A Moore neighborhood with $r = 1$ includes 8 neighbors; with $r = 2$, the neighborhood extends radially: there are 24 neighbors.

In an effort to eliminate isolated Normal vHPCs and reduce the nonbiomimetic columnar features, we extended the preceding explorations using $r = 2$ neighborhoods by adding a requirement that 2 (and subsequently 4) lateral neighbors must have initiated Necrosis-Triggered. Doing so reduced the columnar features and further skewed the average location of Necrosis-Triggered events toward the CV, but also reduced the total number of Necrosis-Triggered and Necrotic events. The patterns caused us to question a specification carried forward from much earlier work: vHPCs occupy only 90% of grid points. During earlier work, we had envisioned placing other Cell types on the vacant grid points. Adding vHPCs to all grid points increased number of early Necrosis-Triggered events and subsequent Necrotic events. Moore neighborhoods had more Necrosis-Triggered events at later times adjacent to the CV. The change also reduced differences in outcomes when using the larger $r = 2$ neighborhoods versus $r = 1$ neighborhoods. Because of the increased outcome similarity, we focused more on the smaller $r = 1$ neighborhood. Also, instead of requiring downstream *and* lateral Necrosis-Triggered neighbors, we relaxed the requirement to one *or* the other. Those refinements produced further incremental progress toward the objective.

We implemented the PC snapshot animations in part to help generate ideas for further improvements. Upon inspection of the first batch, we observed the emergence of a nonbiomimetic Necrotic "V" pattern: more Necrotic vHPCs were consistently piling-up at the lateral edges of the 2D SS snapshot grid. We hypothesized that delivery of vAPAP from upstream SSes to the leading grid points in each Layer 3 SS (top row in PC animations) was not random. We overcame that bias by rewriting the *tryRim()* method in *SS.java* to eliminate any delivery bias. Initial snapshots also showed that there were more Necrotic events than Necrosis-Triggered events. The cause was a coding error. The error was corrected and cycling through the IR Protocol continued. We explored reducing the number requirement for lateral and/or downstream neighbors. For some experiments, reductions did not significantly alter temporal patterns.

Experiments Using Test Mice

Recorded measurements are from experiments on two variants of Test Mice, both employing the logic in Figure 6. One employs the von Neumann neighborhood; the other employs the Moore

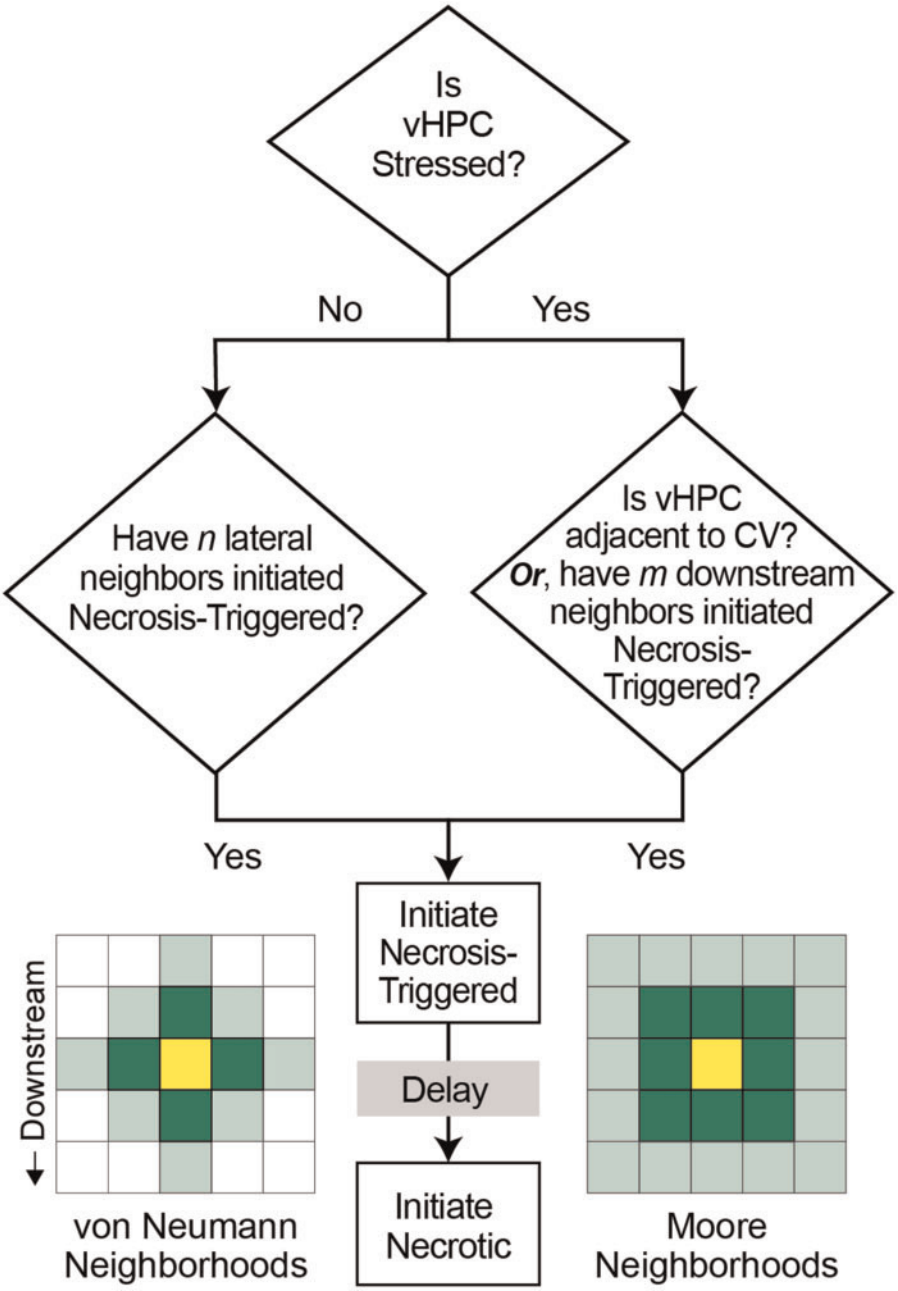

Figure 6. Logic used each simulation cycle by Test Mouse vHPCs to decide to initiate (or not) Necrosis-Triggered. Whether a vHPC is Stressed mediates the logic. After initiating Necrosis-Triggered, the vHPC schedules transition-to-Necrotic to occur following a randomly specified delay. Moore and von Neumann neighborhoods are illustrated relative to the center decision-making vHPC. Darker vHPCs: neighborhood with a $r = 1$ Manhattan radius; darker + lighter vHPCs: neighborhood with a $r = 2$ Manhattan radius. For the results in Figures 7 and 8, $n = 2$, $m = 1$, and $r = 1$.

neighborhood. Their Figure 2C model mechanisms use identical specifications. Consequently, measurements of many vAPAP Disposition, Metabolism, and Toxicity features during these two experiments along with those from Control Mouse experiments were indistinguishable because entities and events preceding breaching the Necrosis Threshold (Control experiments) or Stressed Threshold (Test experiments) are the same. An example is the amount of vAPAP in Mouse Body (maps quantitatively to APAP blood levels in mice) in Figure 7A. The data are from the experiment on Test Mice employing von Neumann-based logic. At the resolution of the data, vAPAP measurements from Test Mice using Moore-based logic and from Control Mice are indistinguishable (superimposable). Location-dependent per-vHPC amounts of vAPAP, NAPQI, and cumulative GSH Depletion (as in Figure 5) from experiments on Controls and Test Mice were comparable.

Figure 6 logic employed by Test Mice specifies that to initiate Necrosis-Triggered, a Stressed vHPC must be either adjacent to CV or have one downstream neighbor that has initiated Necrosis-Triggered. A Normal vHPC must initiate Necrosis-Triggered when its two lateral neighbors have initiated Necrosis-Triggered.

The following is an example of a sequence of events that can occur. (1) At the end of simulation cycle t, a vHPC is Stressed. It

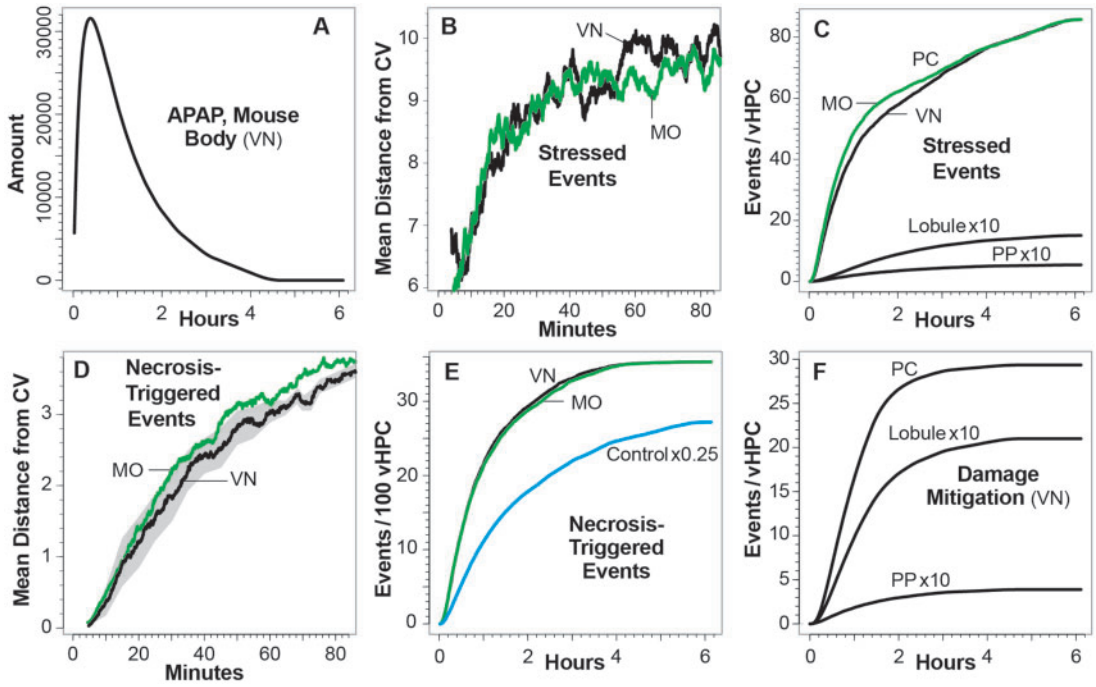

Figure 7. Test Mice: spatiotemporal measurements of intra-vHPC events. Each vHPC utilizes information acquired from neighbors in following the logic in Figure 6 with $n = 2$ and $m = 1$. Results are from two independent experiments, during which only the $r = 1$ neighborhoods in Figure 6 are used. Experiment 1: each vHPC acquires information from neighbors within its von Neumann (VN) neighborhood. Experiment 2: each vHPC acquires information from neighbors within its Moore (MO) neighborhood. Distances from CV for Stressed and Necrosis-Triggered events are 181-point centered moving averages. A, APAP amounts in Mouse Body from Experiment 1. Results from Experiment 2 are identical. B, Average location of Stressed vHPCs each simulation cycle. C, Cumulative Stressed events per vHPC from Experiment 2. Lobule, PP, and PC are as specified in Figure 5. At this resolution, Lobule and PP data from Experiment 2 are indistinguishable. D, Average location each simulation cycle of vHPCs that have initiated Necrosis-Triggered. Necrosis-Triggered always occurs first in vHPCs adjacent to the CV (see Supplementary Videos S2-S6). The gray-shaded area spans ± 1SD (at 2.5–5 min intervals) for the von Neumann neighborhood in Experiment 1. E, Cumulative Necrosis-Triggered events per 100 vHPCs. Corresponding data from Control vHPCs are provided for comparison. Because many Stressed vHPCs did not meet the logic conditions during Test Mouse experiments, cumulative Necrosis-Triggered events during the latter are only about 29% of those that occurred during the Control Mouse experiment. F, Cumulative Damage mitigation events from Experiment 1. At this resolution, corresponding data from Experiment 2 is indistinguishable.

has one adjacent lateral neighbor that is Necrosis-Triggered (but no downstream neighbor is Necrosis-Triggered). (2) At the end of simulation cycle $t+1$, because its mitoD count has dropped, it has reverted to Normal. Also, during simulation cycle $t+1$, a second lateral neighbor has initiated Necrosis-Triggered. (3) Although the vHPC is Normal, during simulation cycle $t+2$, it initiates Necrosis-Triggered.

The moving averages for the mean location of Stressed events (Figure 7B) are necessarily similar to the corresponding distance-from-CV measurements for Necrosis-Triggered in Figure 5B. That is because the criterion for initiating Stressed and Necrosis-Triggered are the same. We observed no significant difference between cumulative Stressed events for Test Mice using von Neumann- and Moore-based logic (Figure 7C). The significant difference in per-vHPC cumulative number of Stressed events within PC and PP bands is a consequence of dramatic differences in per-vHPC mitoD amounts; see Figure 5E. Per-vHPC mitoD amounts are mostly the same for Test and Control Mice.

There are sharp differences between moving averages for the mean distance from the CV of Necrosis-Triggered events in Test (Figure 7D) and Control Mice (Figure 5B). In Test Mice, those averages start at the CV and stay tightly clustered as the location advances upstream from the CV. The phenomenon is illustrated in Figure 8 and Supplementary Videos 2–6. The cumulative numbers of Necrosis-Triggered events (Figure 7E) for both Test Mice are virtually indistinguishable. It is noteworthy that those values are dramatically smaller than corresponding Control Mice values. In Control Mice, some Necrosis is triggered considerably upstream of the CV. At 6 h during each trial, several vHPCs in Lobular Layer 2, along with fewer in Layer 1, have initiated Necrosis-Triggered. In experiments on Test Mice (for the Dose used), there were no Necrosis-Triggered events in Layers 1 and 2.

At the resolution of the Damage Mitigation event data (Figure 7F), measurements from Test Mice using von Neumann- and Moore-based logic are indistinguishable, which is evidence that the logic used has no cumulative influence on other Figure 2C events.

Pericentral Snapshot Animations

Figure 8 presents a sequence of images from Supplementary Video 2 recorded from one Layer-3 SS during one trial of a 12-trial experiment. The images convey a reasonable impression of how events unfolded during an experiment that employs von Neumann-based logic. After 6 h, all vHPCs adjacent to CVs were Necrotic in all 12 trials. Eight snapshots show no Stressed vHPCs. It may seem surprising that Stressed vHPCs are so sparse. However, during the illustrated experiment, 25 999 vHPC entered Stressed status. Because mitoD is being generated and depleted (by Damage Mitigation) before depletion of vAPAP, it is possible for a vHPC to transition from Normal to Stressed to Normal more than once. Note the Stressed vHPC at 1.92 h. There is a Necrosis-Triggered vHPC downstream, but because this Test Mouse is employing von Neumann-based logic, it does not initiate Necrosis-Triggered. Had this arrangement occurred during

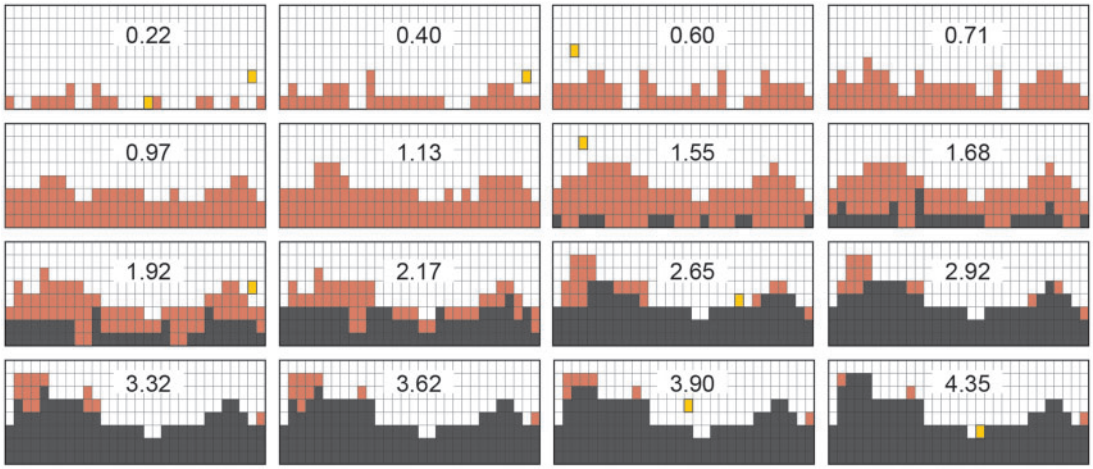

Figure 8. Representative snapshots taken during a single Test Mouse trial. The value on each image is the time (hours) after Dosing when each image was recorded. Data were recorded from one of the three Layer 3 SSes during a single Test Mouse trial. The black-bordered vHPC (often isolated) are Stressed. Light shaded vHPCs are Necrosis-Triggered. Black vHPCs are Necrotic.

the Test Mouse experiment that employed Moore-based logic, that vHPC would have initiated Necrosis-Triggered. Even though this is only a single illustration, one might expect that the Test Mouse experiment employing Moore-based logic could generate more Necrotic events. That is indeed the case: cumulative Necrotic events = 4764 for the Figure 8 experiment, which employed von Neumann-based logic, whereas cumulative Necrotic events = 5449 for the experiment that employed Moore-based logic.

DISCUSSION

The mechanisms utilized by Control Mice (Figs. 2A and 2B) provide a plausible, somewhat coarse grain model of explanation for selected early features of APAP-induced hepatic injury. Other well-documented features and phenomena that become evident after 6 h are not yet addressed. Examples include involvement of the immune system, early disruption of cell-cell tight junctions, mitochondrial autophagy and biogenesis, removal of APAP protein adducts, and hepatocyte proliferation.

Control vHPCs function independent of their neighbors. Because of built-in stochasticity, the average location of Necrosis-Triggered events (gray area, Figure 5B) can shift within and between trials. Consequently, at any time post-Dose, there is no clear demarcation between Necrosis-Triggered vHPCs and vHPCs designated Normal in Figure 2A. The absence of a clear transition is inconsistent with patterns of damage evidenced by the H&E staining (Figure 3) and TUNEL labeling (Figure 4).

By imposing the following two additional target attributes, the Control mechanism from Smith *et al.* (2018) was falsified. (1) The earliest Necrosis-Triggered events occur first adjacent to the CV, and (2) subsequent Necrosis-Triggered events occur primarily adjacent to vHPCs that have already Triggered Necrosis. To achieve those targets, we employed two divergent approaches. The first maintains quasi-autonomous vHPC function; therefore, requiring no inter-vHPC communication. There are multiple ways in which the quasi-autonomous Control mechanism might be refined as part of a strategy to achieve both new targeted attributes. We considered several refinements and discovered that coupling mitoD amplification to the breaching of the GSH Depletion Threshold moved average early Necrosis-Triggered events closer to CV (Supplementary Experiment 7), but did not cause them to start near the CV.

However, a sizable space of candidate model mechanisms remains, in which quasi-autonomous vHPC function is maintained and inter-vHPC communication is not essential, that may achieve the two target attributes within some tolerance. An exploratory tuneable resolution approach (Kirschner *et al.*, 2014) can be used to extend the preceding feature coupling strategy to include couplings among additional Figure 2A events, particularly couplings that include Damage Mitigation. Doing so may require synchronizing Lobular location-dependent configurations beyond the five in Figure 2B. However, before proceeding, we must shrink considerably the space of candidate mechanism variants that will be explored. The process of eliminating model mechanisms will require wet-lab evidence capable of eliminating (falsifying) some variants but not others. One source of such evidence could be multiple same-time, same-liver histological sections in which CV-to-PV patterns (or lack thereof) of different relevant macromolecular targets are visualized using immunohistochemical staining methods. Another source of evidence might come from necessary improvements in one or more of these three advanced technologies: (1) Using matrix-assisted laser desorption/ionization mass spectrometry imaging (MALDI MSI) to obtain spatiotemporal visualizations of the intrahepatic distribution of selected macromolecules, as done recently with APAP metabolites and protein adducts (Sezgin *et al.*, 2018). (2) Resolving intralobular coordinates for specific sets of liver genes based on zonation of landmark genes (Halpern *et al.*, 2017). (3) Classifying relative expression levels of selected macromolecules in PP and PC lobular sections obtained by laser microdissection, as done by Tachikawa *et al.* (2018) for drug transporters and metabolizing enzymes.

Ample wet-lab evidence supports the pursuit of Control mechanism modifications that use an analogy of intracellular communication to achieve the two target attributes. Communication through gap junctions is the most straightforward and direct (Asamoto *et al.*, 2004). Evidence suggests that it can facilitate and counteract hepatic cell death processes (Decrock *et al.*, 2009). APAP-induced necrosis is modulated by attached cells via gap junctions (Saito *et al.*, 2014). Maes *et al.* (2017) report that blocking connexin hemichannels reduces

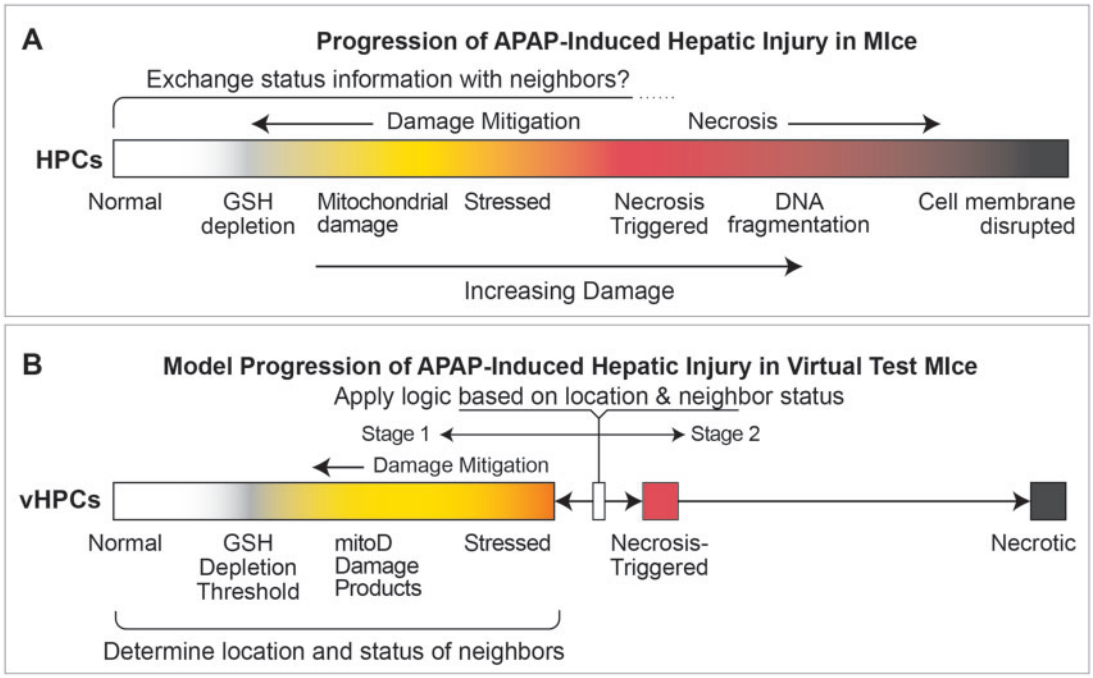

Figure 9. The progression of features characterizing APAP-induced hepatic injury. A, This spectrum depicts APAP-induced hepatic injury *in vivo* as a complex process. Stages of progression are typically identified by a characteristic feature or activity, including those listed. B, This sketch depicts simulated APAP-induced injury in Test Mice as a two-stage sequence. Stage 1 (Normal-to-Stressed) is the coarse grain biomimetic model mechanism described in Figure 2C. During Stage 2, each vHPC determines its ultimate fate by using acquired information about neighbor status and adhering to Figure 6 logic.

measurements of APAP-induced toxicity. On the other hand, genetic ablation of connexin32 does not alter the characteristic features of APAP hepatotoxicity (Maes *et al.*, 2016).

The evidence supporting interhepatocyte exosome-based communication is stronger. Exosomes function within various tissues as intercellular communication vehicles. They deliver a variety of signaling macromolecules between particular cells to modulate or mediate cellular processes (Hirsova *et al.*, 2016; Lai *et al.*, 2015; Tetta *et al.*, 2013). The following are relevant examples. Stress-induced changes in exosome composition can influence the responses of distant cells (Villarroya-Beltri *et al.*, 2014). Exosomes alter the behavior of recipient cells (Lemoinne *et al.*, 2014; Tetta *et al.*, 2013). Within hepatic lobules, exosomes mediate intercellular communication in diseases (Szabo and Momen-Heravi, 2017), and exosome alterations contribute to the pathogenesis of drug-induced liver injury (Holman *et al.*, 2016; Thacker *et al.*, 2018). Changes in exosome content precede hepatocyte necrosis caused by tolvaptan (Mosedale *et al.*, 2018). Significant alterations in hepatocyte-derived exosome production (Duan *et al.*, 2019) and content (Holman *et al.*, 2016) have been reported following subtoxic APAP exposure *in vivo* and *in vitro* (Holman *et al.*, 2016). Exosomes from mice with acute APAP-induced liver injury initiate hepatocyte injury in healthy recipient mice (Cho *et al.*, 2018).

We conjecture that the variety of macromolecules carried by hepatocyte-derived exosomes during the processes illustrated in Figure 9A provides information that influences the recipient hepatocyte's processes causing the emergence of necrotic patterns, eg, those in Figures 3 and 4. A requisite for generating an analogous phenomenon within Test Mice is that each vHPC has ongoing access to information about changes in the status of its neighbor vHPCs during Stage 1 (Figure 9B). We implemented means for vHPCs to acquire the information during each cycle. Stage 2 is the mandatory transition from Necrosis-Triggered to Necrotic following a Monte Carlo-sampled time lag.

In Control Mice, vHPCs are either Normal, Necrosis-Triggered, or Necrotic (Figure 2A). During early explorations, we realized we needed a Stressed status (Figure 2C) and that a Stressed vHPC would need to use neighbor status information when considering whether it will initiate Necrosis-Triggered. After exploring several different rule combinations and information-use options (Supplementary Figure 1), we concluded that it would also be necessary to require that a non-Stressed vHPC initiate Necrosis-Triggered when it is flanked by $n = 2$ vHPCs that have already initiated Necrosis-Triggered. When vHPCs execute the resulting mechanism (Figure 2C) and apply the logic in Figure 6 within the two-stage process (Figure 9B), the evidence in Figures 7, 8, and Supplementary Videos 2–6 shows that Necrosis-Triggered events always occur first adjacent to the CV and then spread periportally adjacent to vHPCs that have already initiated Necrosis-Triggered. A consequence is that the variance in location of Necrosis-Triggered events is reduced sufficiently (the gray area in Figure 7D compared with the gray area in Figure 5B) to make clearly evident when and where the transition from Stage 1 to Stage 2 vHPCs occurs.

Although no wet-lab evidence is specifically supportive at comparable levels of granularity, we hypothesize that the two-stage process depicted in Figure 9B is strongly analogous to the actual progression of APAP-induced hepatic injury illustrated in Figure 9A. It can stand as a plausible explanatory theory until contradictory wet-lab evidence is published. However, becoming Necrosis-Triggered (and subsequently Necrotic) is not a seamless continuation of an unfolding model mechanism. Instead, the transition is a product of applying the logic in Figure 6, and that logic is a placeholder for a yet-to-be-posited, concrete virtual communication mechanism.

The model mechanism utilized by Test Mice and the one above (Supplementary Experiment 7), which strove to achieve the two new target attributes by making intra-vHPC events coupled and incrementally more interconnected and detailed, are presented as being divergent approaches. Reality may map to a convergence of those mechanisms in which a primary role of interhepatocyte communication is to tightly coordinate and maintain hepatocyte processes based in part on relative PV-to-CV location, thereby minimizing the variance of hepatotoxicity attributes of collocated hepatocytes.

Direct validation evidence is needed to strengthen the credibility for a more explanatory communication-enabled model mechanism. A logical next step in acquiring that evidence is to develop an alternative to the Test Mouse mechanism in Figure 2C in which each individual vHPC generates and exports concrete objects that contain necessary information on its current status—call it vMouse-2. Neighboring vHPCs would be able to recognize those objects, distinguish them from other mobile objects, such as vAPAP and its Metabolites, internalize them (or not) and the contained information would (or not) influence ongoing processes. The objects generated by a vMouse-2 mechanism would be intentionally analogous to exosomes. A vMouse-2 mechanism could be discovered and developed scientifically using cross-model validation, with Test Mouse phenomena as referents. Quantitative validation targets for use during IR Protocol cycles would come from measurements of Test Mouse phenomena, such as those in Figures 7 and 8. Once cross-model validation targets are achieved, efforts can begin to establish mappings between the dynamics of virtual exosomes along with the information that they contain, and (1) direct quantitative measurements of exosomes, (2) the molecular signals contained in those exosomes, and (3) the intracellular pathways that those signals influence.

SUPPLEMENTARY DATA

Supplementary data are available at *Toxicological Sciences* online.

FUNDING

M.R.M. is supported in part by the Pinnacle Research Award from the AASLD Foundation. R.C.K. and A.K.S. are supported in part by the UCSF BioSystems Group. Tempus Dictum, Inc. supported GEPR's effort but imposed no commercial restrictions or constraints. H.J. is supported by National Institutes of Health (R01 DK102142).

DECLARATION OF CONFLICTING INTERESTS

The author(s) declared no potential conflicts of interest with respect to the research, authorship, and/or publication of this article.

ACKNOWLEDGMENTS

We thank the authors of the MASON simulation toolkit and also the creators of the SimTK project-hosting platform for facilitating development and distribution of this project.

REFERENCES

Asamoto, M., Hokaiwado, N., Murasaki, T., and Shirai, T. (2004). Connexin 32 dominant-negative mutant transgenic rats are resistant to hepatic damage by chemicals. *Hepatology* **40,** 205–210.

Cho, Y. E., Seo, W., Kim, D. K., Moon, P. G., Kim, S. H., Lee, B. H., Song, B. J., and Baek, M. C. (2018). Exogenous exosomes from mice with acetaminophen-induced liver injury promote toxicity in the recipient hepatocytes and mice. *Sci. Rep.* **8,** 16070.

Darden, L. (2008). Thinking again about biological mechanisms. *Philos. Sci.* **75,** 958–969.

Decrock, E., Vinken, M., De Vuyst, E., Krysko, D. V., D'Herde, K., Vanhaecke, T., Vandenabeele, P., Rogiers, V., and Leybaert, L. (2009). Connexin-related signaling in cell death: To live or let die? *Cell Death Differ.* **16,** 524.

Du, K., Ramachandran, A., McGill, M. R., Mansouri, A., Asselah, T., Farhood, A., Woolbright, B. L., Ding, W. X., and Jaeschke, H. (2017). Induction of mitochondrial biogenesis protects against acetaminophen hepatotoxicity. *Food Chem. Toxicol.* **108**(Pt A), 339–350.

Duan, L., Ramachandran, A., Akakpo, J. Y., Weemhoff, J. L., Curry, S. C., and Jaeschke, H. (2019). Role of extracellular vesicles in release of protein adducts after acetaminophen-induced liver injury in mice and humans. *Toxicol. Lett.* **301,** 125–132.

Gujral, J. S., Knight, T. R., Farhood, A., Bajt, M. L., and Jaeschke, H. (2002). Mode of cell death after acetaminophen overdose in mice: Apoptosis or oncotic necrosis? *Toxicol. Sci.* **67,** 322–328.

Halpern, K. B., Shenhav, R., Matcovitch-Natan, O., Tóth, B., Lemze, D., Golan, M., Massasa, E. E., Baydatch, S., Landen, S., Moor, A. E., *et al.* (2017). Single-cell spatial reconstruction reveals global division of labour in the mammalian liver. *Nature* **542,** 352–356.

Hirsova, P., Ibrahim, S. H., Verma, V. K., Morton, L. A., Shah, V. H., LaRusso, N. F., Gregory, J., Gores, G. J., and Malhi, H. (2016). Extracellular vesicles in liver pathobiology: Small particles with big impact. *Hepatology* **64,** 2219–2233.

Holman, N. S., Mosedale, M., Wolf, K. K., LeCluyse, E. L., and Watkins, P. B. (2016). Subtoxic alterations in hepatocyte-derived exosomes: An early step in drug-induced liver injury? *Toxicol. Sci.* **151,** 365–375.

Hu, J., Ramshesh, V. K., McGill, M. R., Jaeschke, H., and Lemasters, J. J. (2016). Low dose acetaminophen induces reversible mitochondrial dysfunction associated with transient c-Jun N-terminal kinase activation in mouse liver. *Toxicol. Sci.* **150,** 204–215.

Hunt, C. A., Erdemir, A., Mac Gabhann, F., Lytton, W. W., Sander, E. A., Transtrum, M. K., and Mulugeta, L. (2018). The spectrum of mechanism-oriented models for explanations of biological phenomena. *Processes* **6,** 56.

Hunt, C. A., Kennedy, R. C., Kim, S. H., and Ropella, G. E. P. (2013). Agent-based modeling: A systematic assessment of use cases and requirements for enhancing pharmaceutical research and development productivity. *Wiley Interdiscip. Rev. Syst. Biol. Med.* **5,** 461–480.

Hunt, C. A., Ropella, G. E., Lam, T. N., Tang, J., Kim, S. H., Engelberg, J. A., and Sheikh-Bahaei, S. (2009). At the biological modeling and simulation frontier. *Pharm. Res.* **26,** 2369–2400.

Hunt, C. A., Ropella, G. E., Yan, L., Hung, D. Y., and Roberts, M. S. (2006). Physiologically based synthetic models of hepatic disposition. *J. Pharmacokin. Pharmacodyn.* **33,** 737–772.

Illari, P. M., and Williamson, J. (2012). What is a mechanism? Thinking about mechanisms across the sciences. *Eur. J. Philos. Sci.* **2,** 119–135.

Kirschner, D. E., Hunt, C. A., Marino, S., Fallahi-Sichani, M., and Linderman, J. J. (2014). Tuneable resolution as a systems biology approach for multi-scale, multicompartment computational models. *Wiley Interdiscip. Rev. Syst. Biol. Med.* **6,** 289–309.

Lai, R. C., Yeo, R. W., and Lim, S. K. (2015) Mesenchymal stem cell exosomes. *Semin. Cell Dev. Biol.* **40,** 82–88.

Lemoinne, S., Thabut, D., Housset, C., Moreau, R., Valla, D., Boulanger, C. M., and Rautou, P. E. (2014). The emerging roles of microvesicles in liver diseases. *Nat. Rev. Gastroenterol. Hepatol.* **11,** 350–361.

Luke, S., Cioffi-Revilla, C., Panait, L., Sullivan, K., and Balan, G. (2005). MASON: A multiagent simulation environment. *Simulation* **81,** 517–527.

Macal, C. M., and North, M. J. (2010). Tutorial on agent-based modelling and simulation. *J. Simul.* **4,** 151–162.

Maes, M., McGill, M. R., da Silva, T. C., Lebofsky, M., de Araújo, C. M. M., Tiburcio, T., Pereira, I. V. A., Willebrords, J., Yanguas, S. C., Farhood, A., *et al.* (2016). Connexin32: A mediator of acetaminophen-induced liver injury? *Toxicol. Mech. Meth.* **26,** 88–96.

Maes, M., Yanguas, S. C., Willebrords, J., Weemhoff, J. L., da Silva, T. C., Decrock, E., Lebofsky, M., Pereira, I. V., Leybaert, L., Farhood, A., *et al.* (2017). Connexin hemichannel inhibition reduces acetaminophen-induced liver injury in mice. *Toxicol. Lett.* **278,** 30–37.

Miyakawa, K., Albee, R., Letzig, L. G., Lehner, A. F., Scott, M. A., Buchweitz, J. P., James, L. P., Ganey, P. E., and Roth, R. A. (2015). A Cytochrome P450–independent mechanism of acetaminophen-induced injury in cultured mouse hepatocytes. *J. Pharmacol. Exp. Ther.* **354,** 230–237.

Mosedale, M., Eaddy, J. S., Trask, O. J., Jr, Holman, N. S., Wolf, K. K., LeCluyse, E., Ware, B. R., Khetani, S. R., Lu, J., Brock, W. J., *et al.* (2018). miR-122 release in exosomes precedes overt tolvaptan-induced necrosis in a primary human hepatocyte micropatterned coculture model. *Toxicol. Sci.* **161,** 149–158.

Mulugeta, L., Drach, A., Erdemir, A., Hunt, C. A., Horner, M., Ku, J. P., Myers, J. G., Jr, Vadigepalli, R., and Lytton, W. W. (2018). Credibility, replicability, and reproducibility in simulation for biomedicine and clinical applications in neuroscience. *Front. Neuroinform.* **12,** 18.

Ni, H. M., McGill, M. R., Chao, X., Du, K., Williams, J. A., Xie, Y., Jaeschke, H., and Ding, W. X. (2016). Removal of acetaminophen protein adducts by autophagy protects against acetaminophen-induced liver injury in mice. *J. Hepatol.* **65,** 354–362.

Ni, H. M., Williams, J. A., Jaeschke, H., and Ding, W. X. (2013). Zonated induction of autophagy and mitochondrial spheroids limits acetaminophen-induced necrosis in the liver. *Redox. Biol.* **1,** 427–432.

Park, S., Kim, S. H., Ropella, G. E. P., Roberts, M. S., and Hunt, C. A. (2010). Tracing multiscale mechanisms of drug disposition in normal and diseased livers. *J. Pharmacol. Exp. Ther.* **334,** 124–136.

Park, S., Ropella, G. E. P., Kim, S. H., Roberts, M. S., and Hunt, C. A. (2009). Computational strategies unravel and trace how liver disease changes hepatic drug disposition. *J. Pharmacol. Exp. Ther.* **328,** 294–305.

Petersen, B. K., and Hunt, C. A. (2016). Developing a vision for executing scientifically useful virtual biomedical experiments. In: *Proceedings of the 2016 Spring Simulation Multiconference. Society for Computer Simulation International*, San Diego, CA, pp. 697–706.

Petersen, B. K., Ropella, G. E. P., and Hunt, C. A. (2016). Virtual experiments enable exploring and challenging explanatory mechanisms of immune-mediated P450 down-regulation. *PLoS One* **11,** e0155855.

Petersen, B. K., Ropella, G. E. P., and Hunt, C. A. (2014). Toward modular biological models: Defining analog modules based on referent physiological mechanisms. *BMC Syst. Biol.* **8,** 95.

Pogson, M., Smallwood, R., Qwarnstrom, E., and Holcombe, M. (2006). Formal agent-based modelling of intracellular chemical interactions. *Biosystems* **85,** 37–45.

Ropella, G. E., Park, S., and Hunt, C. A. (2009). Evaluating an hepatic enzyme induction mechanism through coarse-and fine-grained measurements of an in silico liver. *Complexity* **14,** 28–34.

Saito, C., Shinzawa, K., and Tsujimoto, Y. (2014). Synchronized necrotic death of attached hepatocytes mediated via gap junctions. *Sci. Rep.* **4,** 5169.

Sezgin, S., Hassan, R., Zühlke, S., Kuepfer, L., Hengstler, J. G., Spiteller, M., and Ghallab, A. (2018). Spatio-temporal visualization of the distribution of acetaminophen as well as its metabolites and adducts in mouse livers by MALDI MSI. *Arch. Toxicol.* **92,** 2963–2977.

Smith, A. K., Petersen, B. K., Ropella, G. E. P., Kennedy, R. C., Kaplowitz, N., Ookhtens, M., and Hunt, C. A. (2016). Competing mechanistic hypotheses of acetaminophen-induced hepatotoxicity challenged by virtual experiments. *PLoS Comput. Biol.* **12,** e1005253.

Smith, A.K., Ropella, G.E., Kaplowitz, N., Ookhtens, M., and Hunt, C.A. (2014) Mechanistic agent-based damage and repair models as hypotheses for patterns of necrosis caused by drug induced liver injury. In *Proceedings of the 2014 Summer Simulation Multiconference, Jul. 6 (no. 16)*. Society for Computer Simulation International. https://dl.acm.org/citation.cfm?id=2685633; last accessed February 19, 2019.

Smith, A. K., Xu, Y., Ropella, G. E. P., and Hunt, C. A. (2018). A model mechanism-based explanation of an in vitro-in vivo disconnect for improving extrapolation and translation. *J. Pharmacol. Exp. Ther.* **365,** 127–138.

Szabo, G., and Momen-Heravi, F. (2017). Extracellular vesicles in liver disease and potential as biomarkers and therapeutic targets. *Nat. Rev. Gastroent. Hepatol.* **14,** 455–466.

Tachikawa, M., Sumiyoshiya, Y., Saigusa, D., Sasaki, K., Watanabe, M., Uchida, Y., and Terasaki, T. (2018). Liver zonation index of drug transporter and metabolizing enzyme protein expressions in mouse liver acinus. *Drug Metab. Dispos.* **46,** 610–618.

Tetta, C., Ghigo, E., Silengo, L., Deregibus, M. C., and Camussi, G. (2013). Extracellular vesicles as an emerging mechanism of cell-to-cell communication. *Endocrine* **44,** 11–19.

Thacker, S. E., Nautiyal, M., Otieno, M. A., Watkins, P. B., and Mosedale, M. (2018). Optimized methods to explore the mechanistic and biomarker potential of hepatocyte-derived exosomes in drug-induced liver injury. *Toxicol. Sci.* **163,** 92–100.

Villarroya-Beltri, C., Baixauli, F., Gutiérrez-Vázquez, C., Sánchez-Madrid, F., and Mittelbrunn, M. (2014) Sorting it out: Regulation of exosome loading. *Semin. Cancer Biol.* **28,** 3–13,

Yan, L., Ropella, G. E. P., Park, S., Roberts, M. S., and Hunt, C. A. (2008a). Modeling and simulation of hepatic drug disposition using a physiologically based, multi-agent in silico liver. *Pharm. Res.* **25,** 1023–1036.

Yan, L., Sheihk-Bahaei, S., Park, S., Ropella, G. E. P., and Hunt, C. A. (2008b). Predictions of hepatic disposition properties using a mechanistically realistic, physiologically based model. *Drug. Metab. Disp.* **36,** 759–768.